Heliyon 10 (2024) e28803

Contents lists available at ScienceDirect

Heliyon

journal homepage: www.cell.com/heliyon

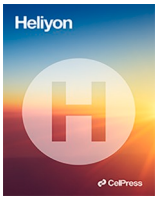

Research article

# Stimulator of interferon genes mediated immune senescence reveals the immune microenvironment and prognostic characteristics of bladder cancer

Zhijun Yao [a], Lin Yang [b], Xiaorong Yang [b], Fang Liu [b], Bin Fu [b,**], Jing Xiong [b,*]

[a] Department of Urology, Hengyang Central Hospital, Hengyang, 421001, China
[b] Department of Urology, First Affiliated Hospital of Nanchang University, Nanchang, 330000, China

ARTICLE INFO

*Keywords:*
STING
SASP
Immune infiltration
Immunotherapy response
Urothelial carcinoma

ABSTRACT

*Background:* Studies have shown that the stimulator of interferon genes (STING) is critical in tumorigenesis, and development. This study aimed to investigate the immune profile and prognostic significance of STING-mediated immune senescence in bladder cancer (BLCA).
*Methods:* We identified differential genes between tumor and normal tissue based on the Cancer Genome Atlas database, and used consensus clustering to identify BLCA subtypes. The genes most associated with overall survival were screened by further analysis and used to construct risk models. Then, comparing the immune microenvironment, tumor mutational load (TMB), and microsatellite instability (MSI) scores between different risk groups. Eventually, a nomogram was constructed based on clinical information and risk scores. The model was validated using receiver operating curves (ROC) and calibration plots.
*Results:* We identified 160 differential genes, including 13 genes most associated with prognosis. Three subtypes of bladder cancer with different clinical and immunological features were identified. Immunotherapy was more likely to benefit the low-risk group, which had higher TMB and MSI scores. The nomogram was found to be highly predictive based on ROC analysis and calibration plots.
*Conclusion:* The risk model and nomogram not only predict the prognosis of BLCA patients but also can guide the treatment.

## 1. Background

A high mortality rate is associated with bladder cancer (BLCA), one of the most prevalent malignancies with high aggressiveness and heterogeneity [1]. Although the efficacy of neoadjuvant therapy based on cisplatin in bladder cancer has been confirmed, overall, the long-term prognosis of bladder cancer patients is still poor [2]. Immune checkpoint inhibitors have been revolutionizing cancer treatment in recent years, resulting in great clinical success for patients who are suffering from advanced cancers [3]. Due to the lack of biomarkers for immunotherapy, only a minority of patients benefit from it [4]. Therefore, finding reliable biomarkers and therapeutic targets is the key issue of immunotherapy for bladder cancer.

* Corresponding author.
** Corresponding author.
*E-mail addresses:* urofbin@163.com (B. Fu), alex7023@126.com (J. Xiong).

https://doi.org/10.1016/j.heliyon.2024.e28803
Received 30 October 2023; Received in revised form 21 March 2024; Accepted 25 March 2024
Available online 26 April 2024

The stimulator of interferon genes (STING) is a key signal transduction molecule of innate immune response in vivo, which is activated by cytoplasmic DNA and plays an important role in regulating the generation of the spontaneous anti-tumor immune response [5]. Cytosolic DNA activates cyclic GMP-AMP (cGAMP) synthase (cGAS) and generates cGAMP, which activates STING and results in the production of type I interferon (IFN). There is increasing evidence that type I IFN is critical for driving effective anti-tumor immunity within the tumor microenvironment [6,7]. Meanwhile, the cGAS-STING pathway is closely related to senescence-associated secretory phenotype (SASP). As cytoplasmic DNA accumulates in senescent cells, cGAS-STING pathway activation occurs, thus stimulating the production of SASP factor, which in turn feeds back to promote cell senescence [8]. Inducing cell senescence is a unique biological consequence of cancer treatment. Therapy-induced senescence can produce SASP that can boost antitumor immunity [9]. Therefore, it is feasible to use STING and SASP-related genes to identify reliable biomarkers for cancer immunotherapy. Furthermore, STING and SASP are key factors in the progression, onset, and treatment of BLCA, according to recent research [10,11].

To help clinicians and BLCA patients make more informed decisions about their treatment, we aim to build a risk model that can accurately predict patient prognosis and immune response by analyzing the relationship between STING and SASP-related genes in BLCA and the immune microenvironment.

## 2. Methods

### 2.1. Datasets

GeneCards database and previously published literature were used to identify STING and SASP-related genes. First, search the GeneCards database for “Stimulator of interferon genes” and " senescence-associated secretory phenotype ", then screen out genes with a relevance score greater than 5, and finally obtain 125 SASP-related genes from Dominik’s research [12]. After sorting, 3370 STING-related genes and 349 SASP-related genes were obtained. We obtained the clinical information of 402 patients and the gene expression data of 425 samples from the cancer genome map (TCGA) database as the training set (6 tumor samples with poor quality were filtered out). The validation set includes the following three queue data. Download IMvigor210 queue data from R package “IMvigor210CoreBiologies”, including complete expression data and clinical information of 348 patients with metastatic urothelial carcinoma receiving ICIs treatment. The data of the E-MTAB-4321 cohort were from the ArrayExpress database (https://www.ebi.ac.uk/biostudies/arrayexpress), including 476 patients with early urothelial carcinoma. We downloaded GSE13507 queue data (167 samples) from the Gene Expression Omnibus database (GEO; https://www.ncbi.nlm.nih.gov/geo) and used annotation files to match probe sequences with gene symbols. All sequencing data are converted to TPM format and processed by log 2 (TPM+1) for subsequent analysis.

### 2.2. Screening target genes

Using the R package “DESeq2″, differentially expressed genes (DEGs) were identified between 406 tumors and 19 normal tissue samples. The filtering standard is $p < 0.05$, $|\log2\text{fold change (FC)}| > 0.585$. For the next step, STING-related genes, SASP-related genes, and DEGs were intersected to identify the target genes. To analyze somatic mutations in BLCA samples, the “maf” file was visualized and processed with the R package “Maftools".

### 2.3. Identify immune subtypes and describe clinical features

To identify different immune subtypes, we used the target genes and the “ConsensusClusterPlus” package to analyze the data of the TCGA cohort. To determine the optimal number of clusters, the consensus matrix was used to calculate the cumulative distribution function (CDF) for each cluster number K. According to the typing results, a comparison was made between immune subtypes in terms of clinical characteristics and survival outcomes.

### 2.4. The immune landscape of different subtypes

TME scores were calculated for each sample using the “estimate” package, which includes immune, stromal, tumor purity, and estimated scores. A variety of immune cells from 22 kinds were measured in each sample using CIBERSORT (https://cibersort.stanford.edu/) to quantify the immune infiltration level. Immune checkpoint and human leukocyte antigen (HLA) gene expression levels are also closely related to the immune microenvironment [13,14], so we compared the levels of their expression among subtypes of the immune system. Further evaluating the differences in immunotherapeutic response between subtypes， we obtained the TIDE score of TCGA-BLCA samples from the online analysis website (http://tide.dfci.harvard.edu/) and verified the analysis results with the real immunotherapeutic data of IMvigor210 cohort.

### 2.5. Construction and validation of the risk signature

The first step was to conduct a Univariate Cox regression analysis to identify genes that were associated with overall survival (OS) ($p < 0.05$). Next, Kaplan-Meier survival analysis was used to determine the model candidate genes most associated with OS. Lastly, the “glmnet” package was used to develop a risk model using the least absolute shrinkage and selector operation (LASSO). Each gene’s

expression level was multiplied by its regression coefficient to calculate a patient's risk score. Samples were divided into low- and high-risk groups based on the median risk score. To evaluate the model's accuracy, K-M survival analysis is performed on the training set and verification set.

### 2.6. Enrichment analysis of different risk groups

We identified DEGs between the low-risk and high-risk groups using the "limma" package. In addition, we downloaded the"c2. cp. kegg.symbols.gmt"annotation file from the molecular signatures database for Gene Set Enrichment Analysis (GSEA).

### 2.7. Predictive value of risk scores for immunotherapy and chemotherapy

To elucidate the association between risk scores and the immune microenvironment, we compared the expression levels of Immunoinhibitor, Immunostimulator, and HLA genes between high and low-risk groups. To characterize the immune profile of the different risk groups, immune cell infiltration abundance and TME scores were also used.

Using the R package "maftools", tumor mutation burden (TMB) was calculated. "cBioPortalData" package was used to download microsatellite instability (MSI) scores from "blca_msk_tcga_2020″, and we selected "MSI_SENSOR_SCORE", which was greater than 0.3 defined as MSI and vice was defined as MSS. Then, We compared the differences between the high-risk and low-risk groups in these aspects of TMB, MSI, and TIDE scores. An analysis of the IMvigor210 cohort's risk scores and the immune response would validate our findings. Additionally, using the "oncoPredict" package [15], we calculated sensitivity scores for each sample to a different drug, with higher scores indicating greater sensitivity. Reference file "GDSC2_Expr (RMA Normalized and Log Transformed). rds" was downloaded from Genomics of Drug Sensitivity in Cancer (https://www.cancerrxgene.org/).

### 2.8. Identification and analysis of key genes

We imported the previously screened target genes into the STRING online analysis website (STRING: functional protein association networks (string-db.org)) for PPI network analysis and screening, and then further identified the core genes of the network in Cytoscape. As screening criteria, 0.7 was set as the minimum interaction score and 20 genes were selected based on the Maximum Neighborhood Component (MNC) algorithm. In the next step, we screened the key model genes. In addition, we performed pan-cancer analysis and immune correlation analysis on the screened genes using the online analysis tools Gene Set Cancer Analysis (GSCA,http://bioinfo.life.hust.edu.cn/GSCA/#/) and the integrated repository portal for tumor-immune system interactions (TISIDB,http://cis.hku.hk/TISIDB/). Finally, to further explore the role of key model genes in the tumor microenvironment, we performed a single-cell level analysis of these genes based on the Tumor Immune Single-cell Hub 2 (TISCH2, ).

### 2.9. Establishment of the nomogram model

To translate our findings into more clinically meaningful analytical tools, we aimed to integrate risk scores and clinical information (age, gender, TNM stage) for each patient to construct a nomogram. By using univariate and multivariate COX regression, we screened independent predictors used to construct the Nomogram. Meanwhile, to validate the predictive value of the models, ROC analysis and plotting of calibration curves were performed on the TCGA-BLCA and GSE13507 datasets to show the predictive power of the models at 1, 3, and 5 years.

### 2.10. Validation of gene expression and protein expressions of key genes

The BLCA tumor cells (T24) and normal bladder cells (SV) were extracted with TRIzol reagent and reverse transcribed with Takara PrimeScript RT. The Shanghai Institute of Cell Biology, Chinese Academy of Sciences (Shanghai, China) provided human BCLA cells. The RT-qPCR was conducted on a Roche LightCycler 96 with an SYBR premixed Ex-Taq kit. Primer sequences are available in the Supplemental Table 1. We calculated the fold change of mRNA using the $2-\Delta\Delta Ct$ method. To confirm that protein levels differed, we also consulted the Human Protein Atlas database (https://www.proteinatlas.org/).

### 2.11. Statistical analysis

R (version 4.2.2) or Graphpad prism (9.0) were used to perform all statistical analyses. All statistical tests were two-sided, if not otherwise stated, and the results were considered statistically significant at a P value of less than 0.05. Wilcoxon rank sum test was used for the comparison of two independent samples, the Kruskal-Wallis test was used for the comparison of multiple samples, and the data were visualized by the "ggplot 2″ package. Through Spearman correlation analysis, we identified the correlation between two continuous variables. Two categorical variables were compared using the chi-square test. The statistical significance of Kaplan-Meier (K-M) survival analysis results was assessed by using the two-sided log-rank test.

## 3. Result

### 3.1. Screening and mutation analysis of target genes (TGs)

Through analyzing the difference in gene expression between bladder tumor tissues and normal tissues, we obtained 7211 DEGs, which were then intersected with 3370 STING-associated genes and 349 SASP-associated genes to finally obtain 160 TGs (Fig. 1A, B). We also plotted volcano maps to visualize the differential expression of TGs, and it can be seen that the distribution of highly and lowly expressed genes in tumor tissues is roughly consistent (Fig. 1C). GO and KEGG analyses demonstrate the biological functions and related pathways enriched by DEGs, mainly focusing on cell proliferation and immune regulation-related pathways (Fig. 1D). To further understand the genomic characteristics of TGs, we analyzed their somatic mutation data. Fig. 1E shows the proportion of TGs mutations in tumor samples and the difference of tumor mutation load by waterfall diagram. Overall, the mutation proportions of these genes were low.

### 3.2. Identification of 4 immune subtypes

We used TGs for co-classification identification with a maximum K value of 6 and 50 repetitions. According to the CDF curves of the consensus score, a k value of 4 is optimal for division (Fig. 2A). As a result, bladder cancer patients were classified into four different immune subtypes. The clinical characteristics of the bladder cancer subtypes are shown in Fig. 2B. We found no significant differences in age and gender among the subtypes, while the distribution of TNM staging was different. Most of the patients in group C1 were at an advanced stage of the disease, while C3 was the opposite. In addition, we analyzed and compared survival differences across subtypes and validated them in different datasets. K-M survival analysis showed significant differences in OS across subtypes in the TCGA-BLCA, IMvigor210, and GSE13507 datasets (Fig. 2C). The E-MTAB-4321 cohort also showed significant associations between subtypes and progression-free survival (PFS) (Fig. 2C). Hence, this suggests to us that TGs play an important role in the development of bladder cancer and deserve to be studied in more depth.

### 3.3. Immune landscape and the immunotherapeutic response

Since the clinical features of the four subtypes are significantly different, it is essential to explore the characteristics of their immune

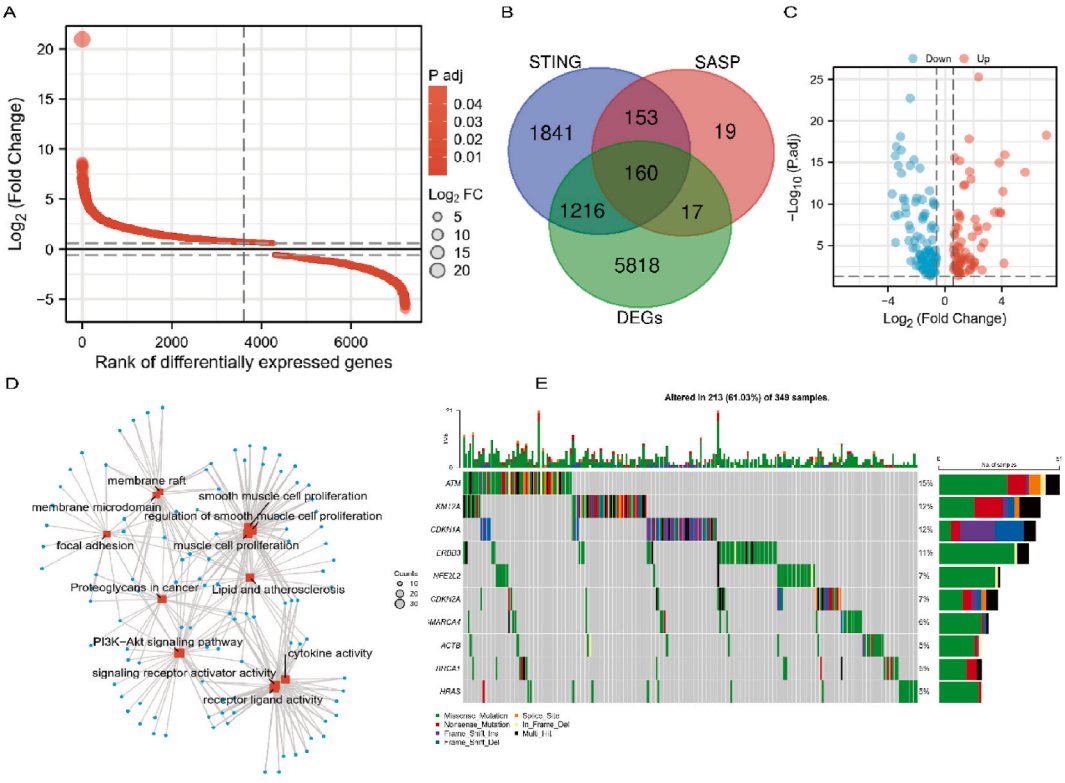


**Fig. 1.** Distribution and mutational characteristics of differential genes in BCLA. (A) Difference ranking diagram of DEGs. (B) Venn diagram of STING, SASP, and DEGs intersecting genes. (C) The volcano plot shows the distribution of differential expression of TGs. (D) Network diagram of GO and KEGG analysis of DEGs. (E) Genomic mutation waterfall plot of TGs in BLCA. Mutation frequencies of the top 10 TGs.

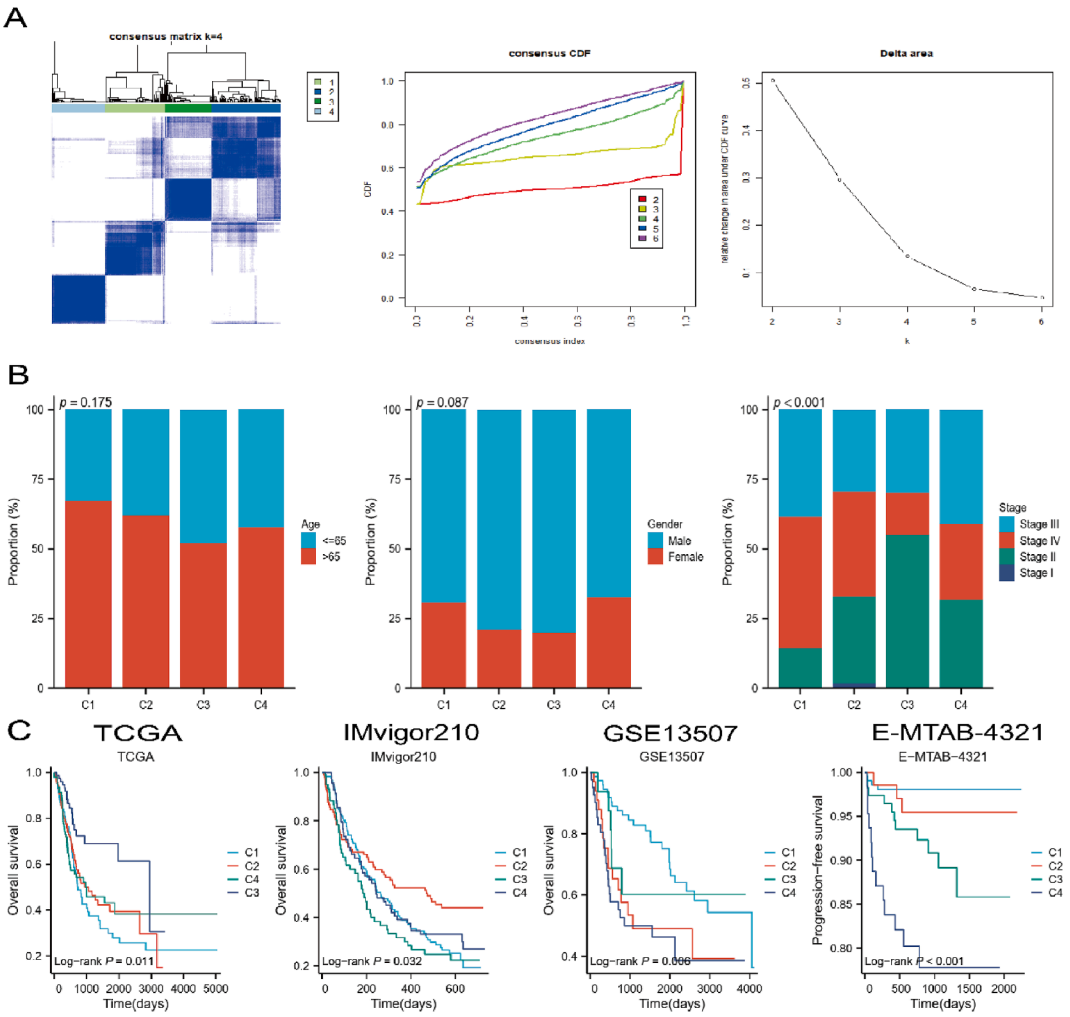


**Fig. 2.** Consensus clustering of TGs in BCLA. (A) Consensus Matrix at K = 4, Consistency Cumulative Distribution Function Plot, and Delta Area Plot. (B) Clinical characteristics of the four subtypes include age, gender, and stage. (C) Kaplan-Meier curves for different subtypes of OS in the TCGA, IMvigor210, and GSE13507 cohort, and the PFS in the E-MTAB-4321 cohort.

microenvironment to understand the inherent heterogeneity of BLCA. In Fig. 3A, we can see that immune scores and stromal scores are higher in C1 and C4 than in C2 and C3, and the opposite is true for tumor purity. Similar expression levels of HLA genes and immune checkpoints were found in C1 and C4 patients, both higher than in C2 and C3 (Fig. 3B, C). As seen in the heat map, both the abundance of immune cell infiltration and cell types differed in different subtypes (Fig. 3D). For example, macrophages infiltrate significantly more in C1 and C4 than in C2 and C3. T cell regulatory (Tregs) and T cell follicular helper (TFH) infiltrate more in C2 and C3, and the role of Tregs in bladder cancer seems to be different from other tumors, as it is associated with a good prognosis and contributes to antitumor immunotherapy [16]. This coincides with our finding that C2 and C3 do have a better prognosis. More promisingly, this was corroborated by our analysis of the differences in immunotherapy response by subtype. In the TCGA cohort (Fig. 3E), C2 and C3 had lower TIDE scores, which means that they were more likely to respond to immune checkpoint inhibitors (ICBs). Similarly, in IMvigor210 with true immunotherapy information, the proportion of immune-responsive patients was significantly higher in C2 than in the other subtypes, which also had the best prognosis (Fig. 3E and .F).

### *3.4. Construction of risk model*

The 4 immune subtypes of bladder cancer identified by TGs differed significantly in terms of clinical features, prognosis, and immune landscape. It is reasonable to assume that the screened TGs may have significant potential in predicting the prognosis and immunotherapeutic response in bladder cancer. Therefore, we screened 45 prognostic genes from 160 TGs (Fig. 4A), 13 of which were most associated with prognosis (Fig. 4B), and they were used to construct a risk model [risk score = MYC * 0.0796 + IGF1 * 0.0218 + SRC*(−0.1188) + PGR*0.0842+RUNX2*0.1344 + CYP1B1*0.0178 + ELN*0.0903 + AXL*(−0.0573) + GSN*0.0346+NOTCH3*0.1267+ADAM17*0.1115+COMP*0.01112 + PGF*0.0531]. Based on the principal component analysis

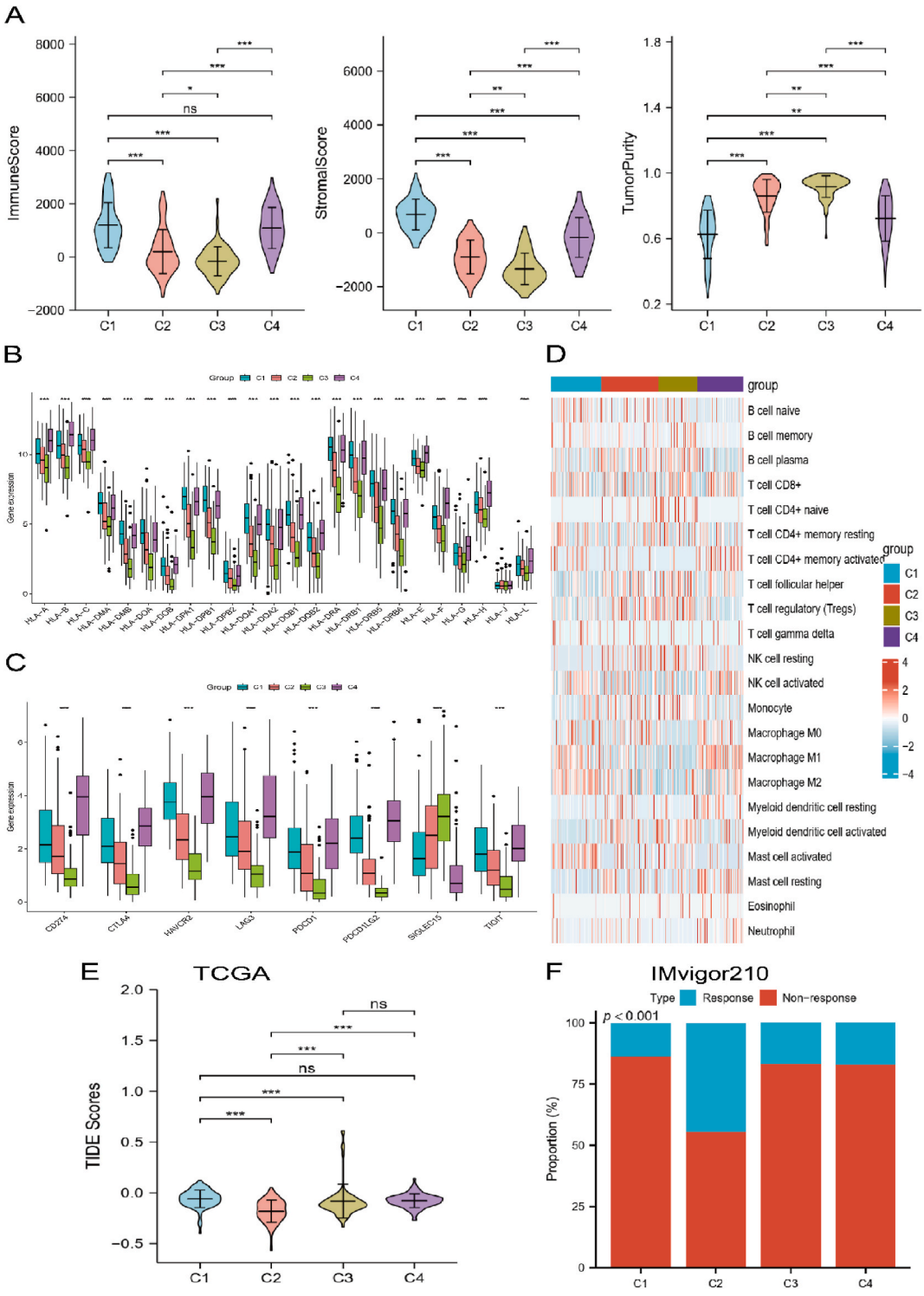


**Fig. 3.** Immune landscape of each subtype. (A) Stromal score, immune score, and tumor purity among the four subtypes. (B) Differential expression of HLA genes and immune checkpoint genes among the four subtypes. (C, D) Heat map of 22 immune cell infiltration differences between the four subtypes. (E) Differences in TIDE scores between subtypes in the TCGA cohort. (F) Response and Non-response to immunotherapy in patients with different subtypes in the IMvigor210 cohort. ns $\geq$ 0.05, * <0.05, ** <0.01, *** <0.001 and **** <0.0001.

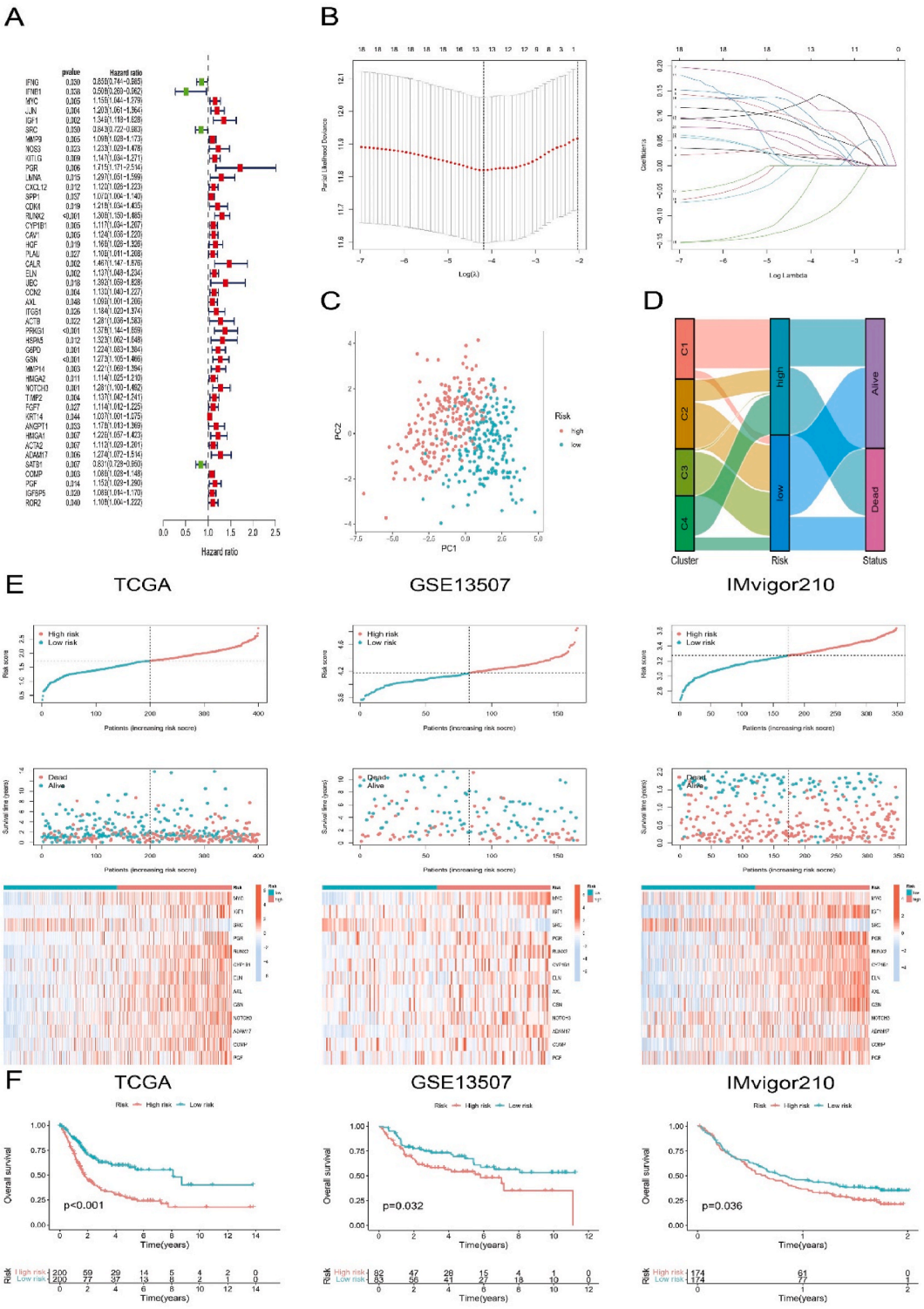


**Fig. 4.** Risk model based on the TCGA cohort. (A) Forest plot of correlation between prognostic genes and OS in the TCGA cohort. Univariate Cox regression analysis was used to determine HR, 95 % CI, and p-value. (B) Cross-validation results of model construction and trajectory changes of prognostic gene coefficients. (C) Results of PCA analysis for high- and low-risk groups. (D) Sankey diagram showing changes in 4 subtypes, risk groupings, and survival status. (E) Classification of patients into high and low-risk subgroups based on median risk scores of TCGA, IMvigor210, and GSE13507; survival status of patients in both subgroups; heat map of 13 prognostic genes. (F) K-M curves of OS in high- and low-risk groups of TCGA, IMvigor210, and GSE13507 cohorts.

(PCA), the risk model can effectively categorize patients into different risk categories (Fig. 4C). Moreover, significant differences in the risk distribution of different immune subtypes can be seen in Fig. 4D. To further verify the accuracy of the model, we analyzed the survival status of the high and low-risk groups in different cohorts. In the TCGA, GSE13507, and IMvigor210 cohorts, the trend of patient survival status with risk score remained highly consistent, and the gene expression distributions in the two groups were similar as well (Fig. 4E). In addition, K-M survival analysis also showed that OS was significantly better in the low-risk group than in the high-risk group (Fig. 4F). However, analysis of E-MTAB-4321 showed no significant difference in progression-free intervals between high and low risk groups ($p = 0.074$), as seen in Supplementary Fig. 1.

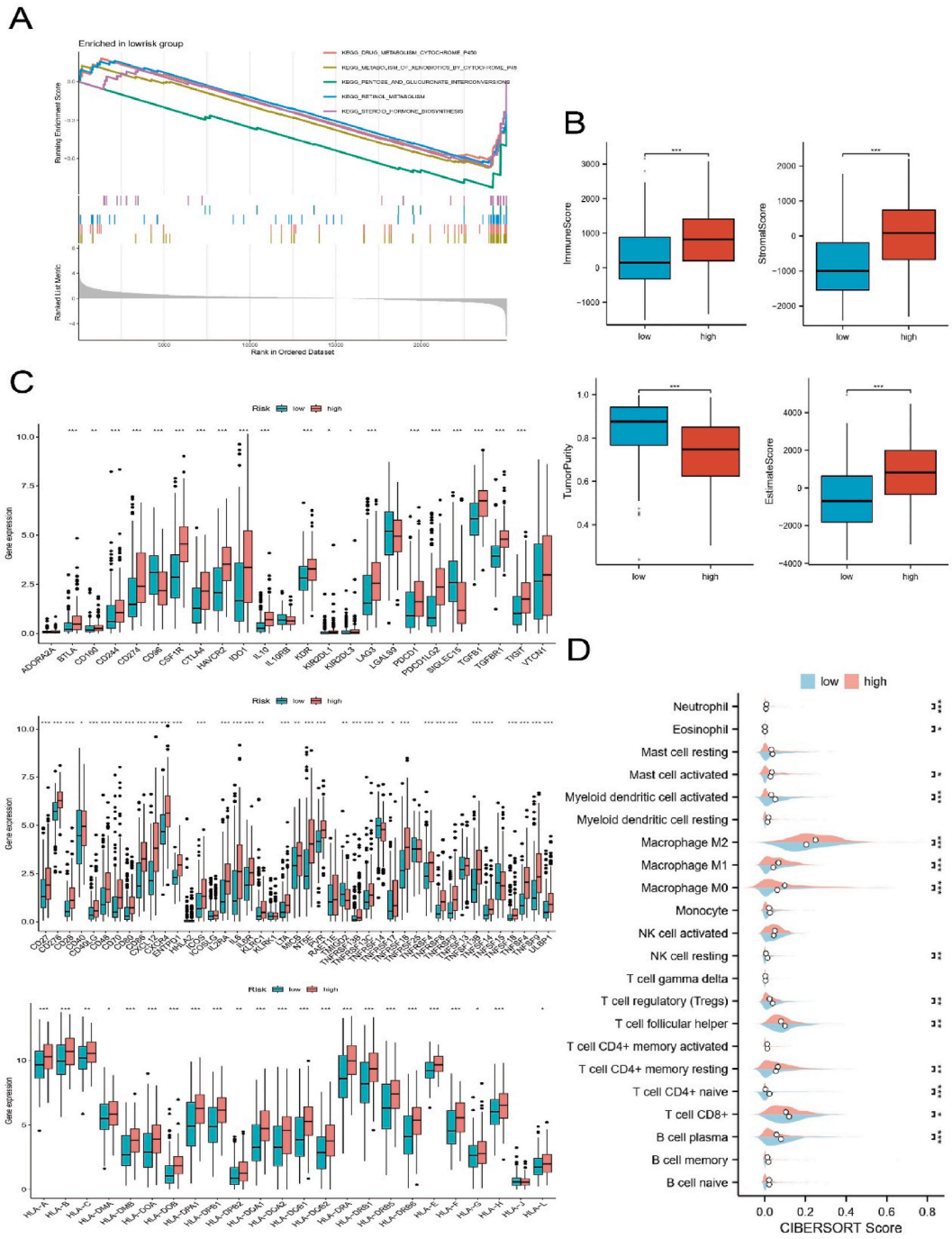


**Fig. 5.** Immune landscape of the high- and low-risk groups. (A) Stromal scores, immune scores, and estimated scores for the high- and low-risk groups. (B) 22 immune cell infiltrates in different risk groups. (C) Expression levels of Immunoinhibitor, Immunostimultor, and HLA genes in different risk groups. (D) Levels of immune cell infiltration in different risk groups. ns ≥ 0.05, * <0.05, ** <0.01, *** <0.001 and **** <0.0001.

### 3.5. Immunological characteristics of the two risk groups

The GSEA results showed that the genes that were highly expressed in the low-risk group were mainly enriched in metabolism-related pathways (Fig. 5A), including pentose and glucuronate interconversions, retinol metabolism, and steroid hormone biosynthesis. Furthermore, a low-risk group had lower immune scores, stromal scores, and estimated scores (Fig. 5B). Based on the level of immune cell infiltration in each sample, we could see that in the low-risk group, there were more abundant plasma cells, CD8 T cells, naive CD4 T cells, activated dendritic cells, TFH and Tregs, while in the high-risk group, there was a higher level of infiltration mainly in macrophages, including macrophages M0, M1, M2 (Fig. 5D). Then, we found that, except for CD96, SIGLEC15, TMIGD2, and TNFRSF14, the expression levels of Immunoinhibitor, Immunostimulator, and HLA genes tended to be lower in the low-risk group (Fig. 5C).

Subsequently, we investigated the inherent relationship between risk scores and immunotherapy effects by using the TMB, MSI, and TIDE scores [17,18]. Those who were low-risk had higher levels of TMB (Fig. 6A). Low-risk patients constituted a greater proportion of the MSI group (Fig. 6B). A lower TIDE score was also achieved by patients in the low-risk group (Fig. 6C). It is reasonable to assume that immunotherapy has a greater likelihood of proving beneficial to patients with low-risk conditions. Encouragingly, the results of the analysis of the IMvigor210 cohort validated our conjecture. In the group that responded to immunotherapy, they had a lower risk score and a higher proportion of patients in the low-risk group (Fig. 6D). In addition, we evaluated the differences in sensitivity of commonly used chemotherapeutic agents in BLCA in different risk groups according to the recommendations of the AJCC guidelines. Low-risk patients were more sensitive to Cisplatin, Vincristine, Paclitaxel, and Epirubicin (Fig. 6E).

### 3.6. Pan-cancer and single-cell sequencing analysis of hub genes

Our PPI network consists of 160 nodes and 875 edges, constructed from the STRING database, which was subsequently imported into Cytoscape software to identify hub genes. The top 20 genes were calculated according to the Degree and MNC algorithms

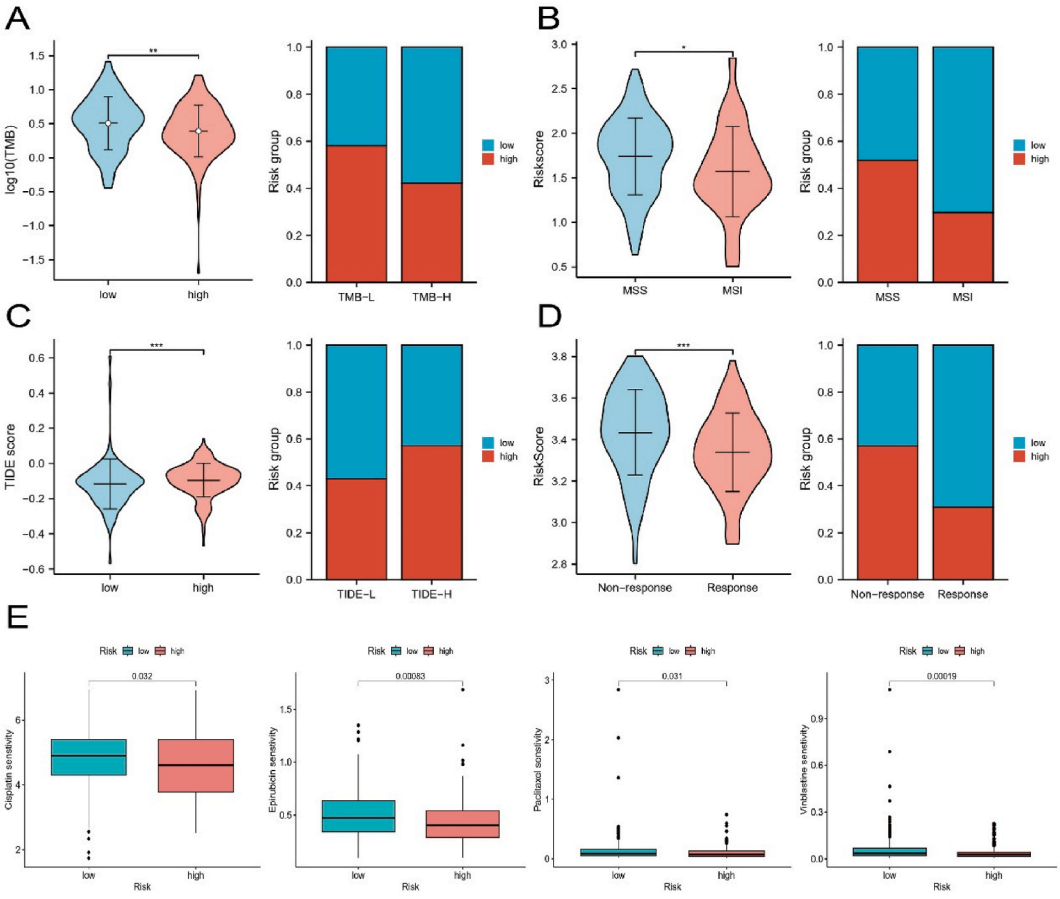


**Fig. 6.** Immunotherapy efficacy and drug prediction. (A) TMB in high and low-risk groups, TMB-L: low TMB; TMB-H: high TMB. (B) Relationship of MSI and MSS with risk scores. (C) TIDE scores in high and low-risk groups, TIDE-L: low TIDE; TIDE-H: high TIDE. (D) Response or Non-response to immunotherapy in the IMvigor210 cohort of patients in different risk groups. (E) Sensitivity of commonly used chemotherapeutic agents for BLCA in high and low-risk groups. ns $\geq$ 0.05, * <0.05, ** <0.01, *** <0.001 and **** <0.0001.

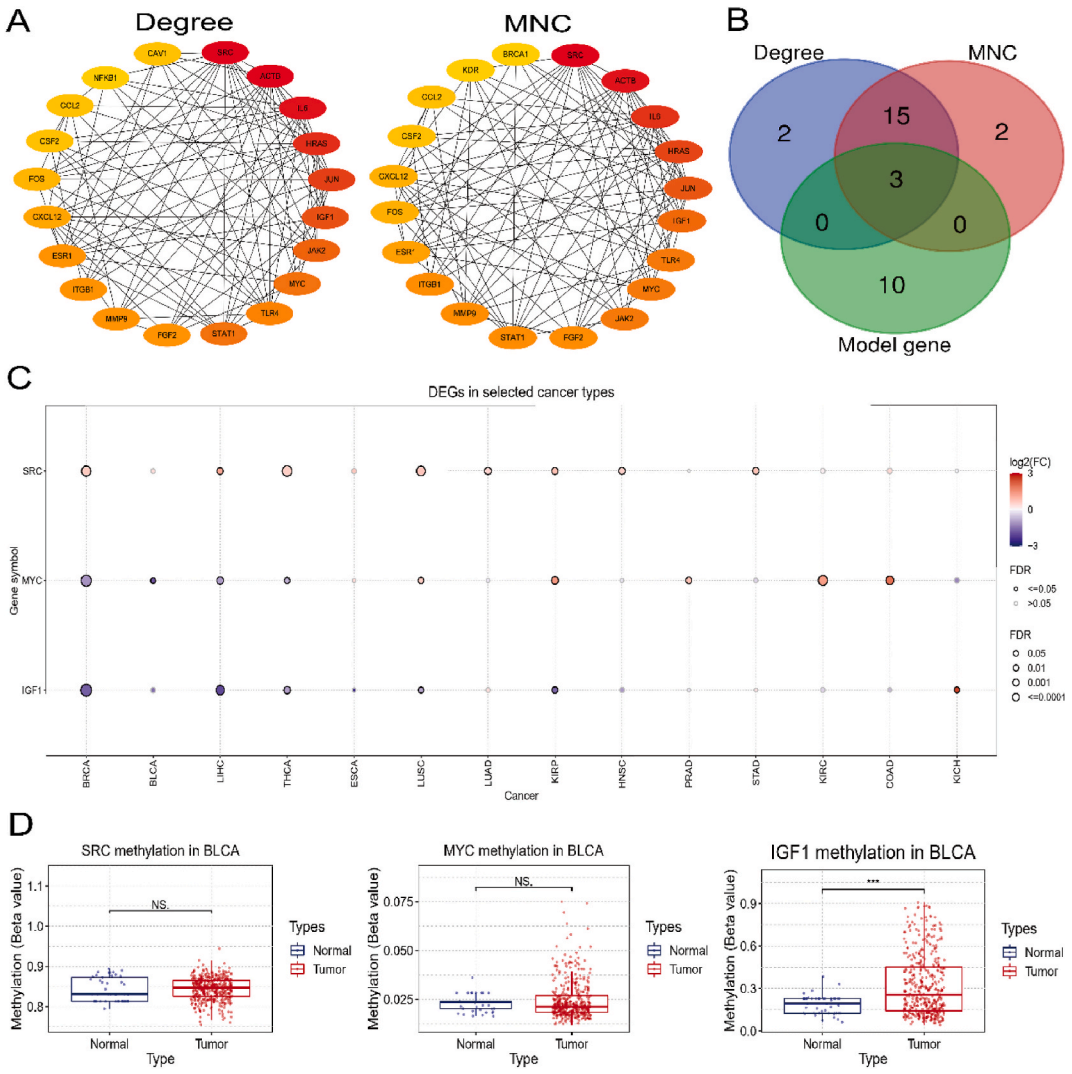


**Fig. 7.** Identification and analysis of key genes. (A) TGs-based PPI network. (B) Degree and MNC algorithm based on top 20 key genes. (C) Venn diagram of the intersection of model genes and top 20 key genes. (D) Methylation levels of SRC, MYC, and IGF1 in tumor and normal tissues. *** <0.001.

(Fig. 7A), and they were intersected with the model genes to obtain three model key genes (Fig. 7B), namely SRC, MYC, and IGF1. Gene expression patterns and prognostic features of key genes were assessed using the GSCA online tool. As shown in Fig. 7C, SRC was highly expressed in tumor samples from most cancers, while IGF1 was the opposite. MYC showed inconsistent expression patterns in different cancers, for example, it showed low expression in BRCA and BLCA, while it showed high expression in KIRC and COAD. Subsequently, we found that the methylation level of IGF1 was elevated in tumor tissues of BLCA, which might be one of the reasons for its reduced expression level, while there was no significant difference between SRC and MYC (Fig. 7D). Next, we focused on the association between IGF1 in BLCA and prognosis and tumor microenvironment.

The expression level of IGF1 was reduced in both unpaired and paired BLCA samples (Fig. 8A). However, we found that IGF1 expression increased with staging and was associated with a poorer prognosis (Fig. 8B), including OS and disease-specific survival (DSS) (Fig. 8C). Subsequently, we found that the role played by IGF1 in bladder cancer immunotherapy studies does not seem to be well understood. Therefore, we used the TISIDB online tool to analyze the link between IGF1 and the immune microenvironment. To begin with, we found that the expression of IGF1 was highly correlated with the immune subtype of cancer, also in BLCA. Based on IGF1 expression, BLCA patients could be classified into six different immune subtypes and there was a strong correlation between them and immune scores (Fig. 8D, E). In addition, we found that IGF1 was positively correlated with most immunoinhibitors, with IL10 having the highest correlation. Among the immunostimulators, IGF1 was negatively correlated with TNFRSF25 (Supplementary Fig. 2A). According to the CIBERSORT score, we found higher levels of infiltration of plasma cells, naive CD4 T cells, and TFH in the IGF1 low expression group (Supplementary Fig. 2B). Meanwhile, IGF1 showed a positive correlation trend with the TIDE score, further suggesting that IGF1 low expression may contribute to immunotherapy (Fig. 8F). Meanwhile, IGF1 showed a positive correlation trend

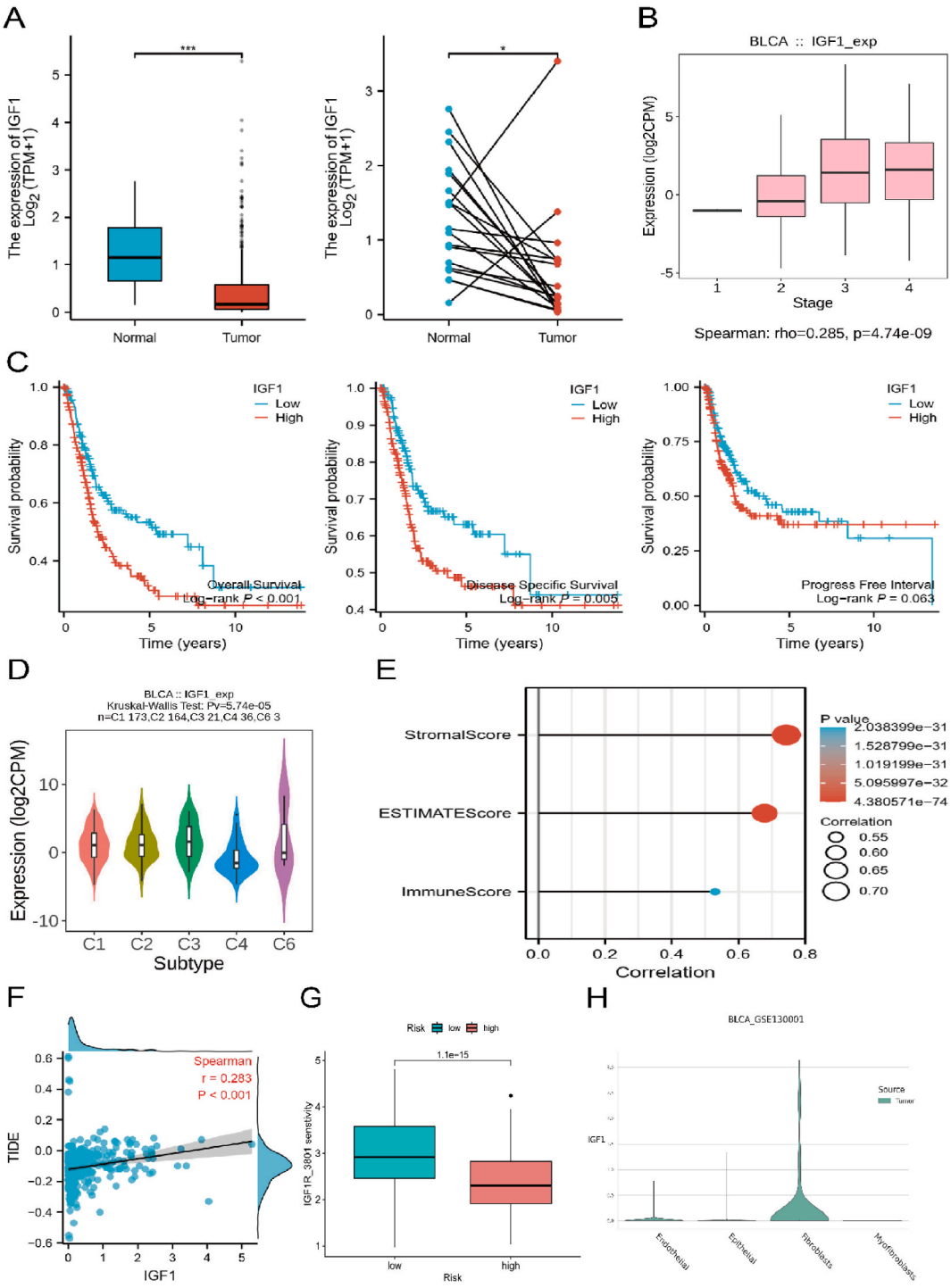


**Fig. 8.** Analysis of key model genes in BLCA. (A) Expression of IGF1 in unpaired and paired samples of BCLA. (B) Association of IGF1 with BLCA stage. (C) K-M curves of IGF1 expression levels in the TCGA-BLCA cohort versus OS, DSS, and Progression Free Intervals. (D) Based on IGF1 expression, BLCA patients can be classified into 6 different immune subtypes. (E) The correlation of IGF1 with the TME Score. (F) The correlation of IGF1 with TIDE score. (G) The sensitivity of IGF1R inhibitors in high and low-risk groups. (H) The results of single cell analysis of IGF1. ns $\geq$ 0.05, * <0.05, ** <0.01, *** <0.001 and **** <0.0001.

with the TIDE score, further suggesting that IGF1 low expression may contribute to immunotherapy. As a coincidence, we discovered that the low-risk group responded better to IGF1R inhibitors, which may have synergistic effects with immunotherapy (Fig. 8G). Lastly, the single-cell analysis revealed that IGF1 expression was concentrated in tumor fibroblast cells (Fig. 8H).

### 3.7. Clinical application of the risk score

In patients with BLCA, stage, age, and risk score were independent predictors of OS (Fig. 9A, B). In the nomogram, the corresponding scores for each prognostic parameter were summed to obtain a total score for each patient, and the higher the score, the worse the prognosis (Fig. 9C). As seen in the calibration plots of the TCGA and GSE13507 cohorts, the predicted probability is almost in a straight line with the actual probability, indicating that the nomogram has reliable predictive performance (Fig. 9D). What's more, the ROC analysis suggests that the nomogram is capable of making accurate predictions. In the training set TCGA cohort, 1-year AUC = 0.723; in the validation cohort GSE13507, 1-year AUC = 0.851 (Fig. 9E).

### 3.8. RT-qPCR and HPA database analysis

The results of SRC, MYC, and IGF1 expression levels in tumor and normal tissues obtained by our RT-qPCR were consistent with the bioinformatics analysis (Fig. 10A, B, C). Furthermore, tumor tissues contained higher levels of SRC and lower levels of MYC protein.

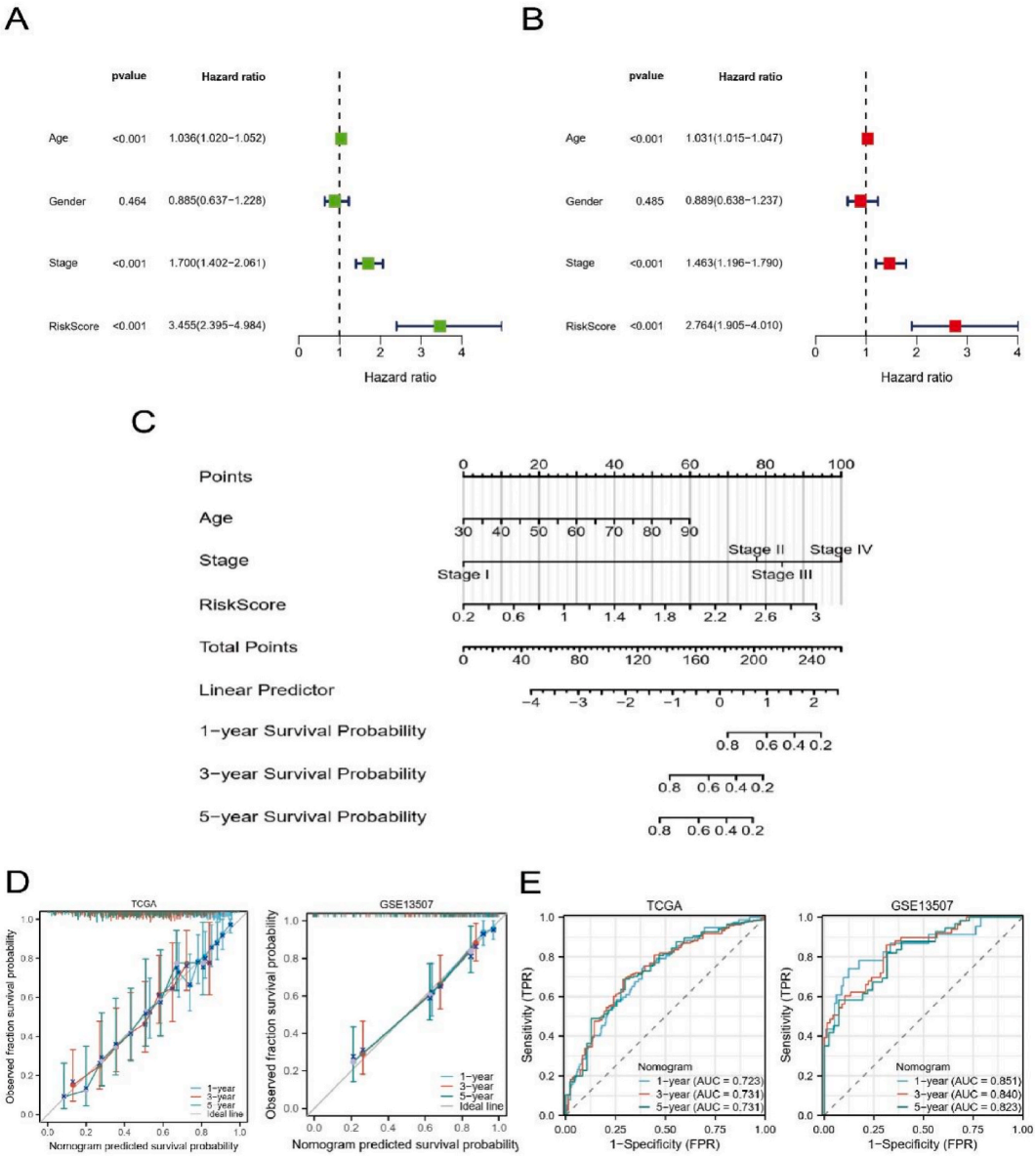


**Fig. 9.** Nomogram of BLCA. (A, B) Univariate and multifactorial analyses containing risk scores and clinical factors. (C) Nomogram for predicting the probability of survival at 1, 3, and 5 years in BLCA patients. (D, E) Calibration plots and time-ROC curves for TCGA and GSE13507 at 1, 3, and 5 years.

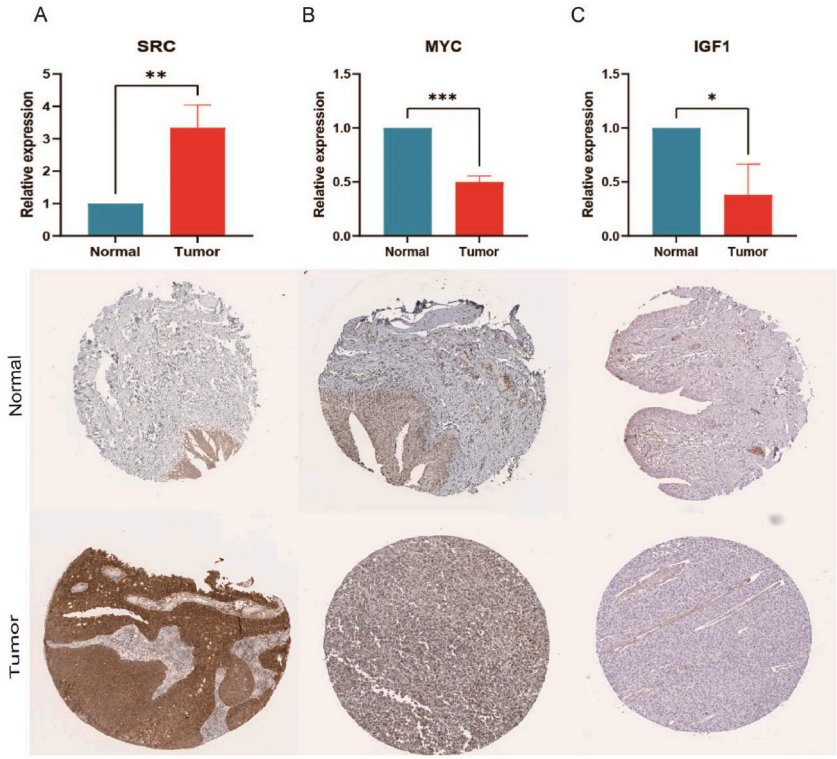


**Fig. 10.** Experimental validation. (A, B, C) Validation of mRNA and protein expression levels of SRC, MYC, and IGF1. * <0.05, ** <0.01, and *** <0.001.

However, IGF1 protein expression was not detected in both tumor and normal tissues, which might be attributed to the lower expression level of IGF1.

## 4. Discussion

The cGAS-STING pathway exerts its antitumor effects by stimulating the patient's immunity, a very attractive feature. Promising experimental results have been obtained with STING agonists, and Huang et al. demonstrated the effect of the STING agonist E7766 against BLCA in vitro and in vivo [19]. More importantly, type I IFNs, which receive cGAS-STING regulation, bridge innate and adaptive immunity. Li et al. believe that cGAS-STING promotes the maintenance of CD8 T cell stemness by regulating the transcription factor TCF1 and relies on type I IFN to enhance the differentiation of stem cell-like CD8 T cells, which is essential for the body's anti-tumor immunity [20]. In addition, recent studies have found that cGAS-STING promotes SASP, which induces immune surveillance and thus exerts tumor-suppressive effects [21]. Consequently, it is crucial to promote cancer cell senescence, induce apoptosis, and increase cytotoxic T cells' protective effects.

Currently, there is no clear connection between the STING and SASP-related genes and the tumor microenvironment in BLCA. A thorough understanding of the intrinsic linkage is essential to guide prognosis and immunotherapy in BLCA. Our study integrated STING and SASP-related genes and identified 160 TGs by differential analysis. After that, we identified 3 subtypes of BLCA with different clinical and immune features, which suggested a close association of these genes with survival and immune microenvironment. Subsequently, 12 prognostic genes most associated with OS were screened and used to construct risk models. We further explored the immune characteristics, drug sensitivity, immunotherapy effects, and prognostic differences in different risk groups.

Our study found higher levels of infiltration of plasma cells, CD8 T cells, naive CD4 T cells, TFH, and Tregs in the low-risk group of patients, while the high-risk group had a high infiltration of macrophages. It is well known that several immune cells other than Tregs and tumor-associated macrophages (TAM) play an active role in the process of antitumor immune effects. When B cells and plasma cells are located in tumors or lymph nodes, they can present antigens to T cells and stimulate their differentiation into cytotoxic T lymphocytes, which then infiltrate into the core or invasive site of the tumor to exert tumor-killing effects. In addition, plasma cells can also produce different types of antibodies to drive different immune responses [22,23]. The role of TFH in the process of the anti-tumor effect of the body is complementary to that of B cells. On the one hand, TFH is important for the formation of germinal centers, and B cells located in germinal centers depend on TFH regulation to differentiate into plasma cells and memory cells, which are the basis for B cells to generate adaptive immunity and immune memory. On the other hand, the recognition of tumor antigens by B cells can promote the development of TFH and enhance the effector function of CD8 T cells to promote anti-tumor immunity through the interaction

between the two [24–26]. Notably, Tregs also present high levels of infiltration, which usually inhibit effective antitumor immunity [27]. However, the findings of Malin et al. overturned our knowledge that Tregs can exert positive antitumor effects in certain malignancies, bladder cancer being one of them [16]. Therefore, The high amount of antitumor cells infiltrating into the tumor may account for a better outcome for patients at low risk. TMB and MSI are reliable biomarkers of the effectiveness of immunotherapy [28]. Palmeri et al. concluded that patients with high levels of TMB and MSI scores tended to have more significant immunotherapeutic effects [18]. Our study further confirms the reliability and feasibility of TMB and MSI as biomarkers. More interestingly, a cisplatin-based chemotherapy regimen may be more effective in the low-risk group. The study by Fu et al. also indicated that cisplatin inhibits bladder cancer proliferation by activating the cGAS-STING pathway [11], which coincides with our findings. In other words, the combination of cisplatin and immunotherapy can produce synergistic antitumor effects.

By identifying 3 key genes through the PPI network, we deeply explored the connection between IGF1 and the immune microenvironment of BLCA. We all know that the IGF family can regulate energy metabolism and growth; they also play an important regulatory role in tumor development [29]. According to our findings, IGF1 expression was associated with poorer BLCA prognosis, and the higher the stage, the higher the expression level. More importantly, IGF1 is closely associated with the immune subtype of BLCA and is a highly promising immunotherapeutic target and biomarker. Although previous studies have proposed IGF1 as a therapeutic target for bladder cancer [30], the relationship between IGF1 and immunotherapy remains unclear. Long et al. found that tumor-associated fibroblasts (CAFs) could lead to BLCA platinum resistance through the activation of IGF1-related pathways [31], and our single-cell analysis also suggested higher IGF1 expression in CAFs. This would suggest that IGF1 could serve as an important bridge for CAFs to influence the BLCA tumor microenvironment. Recent studies point out that CAFs are crucial in shaping the tumor immune microenvironment by secreting various factors that interact with tumor-infiltrating immune cells and other immune components, resulting in tumor cells escaping the immune system [32,33]. As a result, IGF1 is indeed a promising therapeutic target for BLCA, and IGF1R inhibitors may become effective therapeutic agents. Interestingly, the study by Neuzillet et al. has demonstrated that IGF1R inhibitors can inhibit the proliferation of BLCA tumor cells [30]. Perhaps, according to our risk model, the combined application of immunotherapy, cisplatin-based chemotherapy and IGF1R inhibitors to patients in the low-risk group could lead to unexpected therapeutic effects. This provides new ideas for the design of future prospective clinical trials.

In conclusion, our study reveals the clinical and tumor microenvironmental features of BLCA from the perspective of STING and SASP, which are crucial for the prognostic assessment and treatment selection of patients. A model based on 13 prognostic genes aids in predicting the prognosis of BLCA patients and guides subsequent treatment choices. In addition, the nomogram we constructed can accurately predict the OS at 1, 3, and 5 years, which has significant implications for the long-term management of BLCA. Nevertheless, our study still has some shortcomings. To begin with, our study relies mainly on bioinformatics analysis, so further experiments will be required to validate our findings. The second issue is that we derived our model from a retrospective analysis, and high-quality prospective studies are required to enhance its credibility.

## 5. Conclusion

We systematically investigated the molecular characteristics and prognostic potential of STING and SASP-related genes in BLCA and also revealed their intrinsic association with the immune microenvironment. Moreover, the risk model and nomogram we constructed can accurately identify patients' prognoses and enrich the treatment strategies for BLCA. More importantly, we also identified a therapeutic target with significant potential - IGF1.

## Ethics approval and consent to participate

This study has been approved by the Research Ethics Committee of the First Affiliated Hospital of Nanchang University (Nanchang, China). Approval Number: (2022)CDYFYYLK (11–031).

## Consent for publication

All authors agreed to publish this study.

## Availability of data and materials

Our data were obtained from the TCGA database (https://portal. gdc. cancer. gov/), the ArrayExpress database (https://www.ebi.ac.uk/biostudies/arrayexpress), the GEO database (https://www. ncbi. nlm.nih.gov/geo) and the R package "IMvigor210CoreBiologies", and we have uploaded the raw data to the supplementary material.

## Funding

This study was supported by the Key Project of Natural Science Foundation of Jiangxi Province (20212ACB206013), the Youth Project of Natural Science Foundation of Jiangxi Province (20212BAB216037), the Jiangxi Natural Science Foundation (20202BABL206023).

## CRediT authorship contribution statement

**Zhijun Yao:** Writing – review & editing, Writing – original draft, Formal analysis, Data curation. **Lin Yang:** Writing – review & editing, Writing – original draft, Formal analysis, Data curation. **Xiaorong Yang:** Writing – review & editing, Writing – original draft, Formal analysis, Data curation. **Fang Liu:** Formal analysis, Data curation. **Bin Fu:** Conceptualization. **Jing Xiong:** Conceptualization.

## Declaration of competing interest

The authors declare that they have no known competing financial interests or personal relationships that could have appeared to influence the work reported in this paper.

## Acknowledgements

We would like to thank TCGA, GEO, ArrayExpress, and the "IMvigor210CoreBiologies" package for the data provided.

## Appendix A. Supplementary data

Supplementary data to this article can be found online at https://doi.org/10.1016/j.heliyon.2024.e28803.

## References

[1] A.T. Lenis, P.M. Lec, K. Chamie, M.D. Mshs, Bladder cancer: a review, JAMA 324 (19) (2020) 1980–1991, https://doi.org/10.1001/jama.2020.17598.
[2] G. Gakis, Management of muscle-invasive bladder cancer in the 2020s: challenges and perspectives, Eur Urol Focus 6 (4) (2020) 632–638, https://doi.org/10.1016/j.euf.2020.01.007.
[3] S. Bagchi, R. Yuan, E.G. Engleman, Immune checkpoint inhibitors for the treatment of cancer: clinical impact and mechanisms of response and resistance, Annu. Rev. Pathol. 16 (2021) 223–249, https://doi.org/10.1146/annurev-pathol-042020-042741.
[4] G.V. Masucci, A. Cesano, R. Hawtin, S. Janetzki, J. Zhang, I. Kirsch, et al., Validation of biomarkers to predict response to immunotherapy in cancer: volume I - pre-analytical and analytical validation, Journal For Immunotherapy of Cancer 4 (2016) 76.
[5] T. Rivera Vargas, I. Benoit-Lizon, L. Apetoh, Rationale for stimulator of interferon genes-targeted cancer immunotherapy, Eur. J. Cancer 75 (2017) 86–97, https://doi.org/10.1016/j.ejca.2016.12.028.
[6] L.T. Khoo, L.-Y. Chen, Role of the cgas-sting pathway in cancer development and oncotherapeutic approaches, EMBO Rep. 19 (12) (2018), https://doi.org/10.15252/embr.201846935.
[7] V.E. Mekers, V.M. Kho, M. Ansems, G.J. Adema, Cgas/cgamp/sting signal propagation in the tumor microenvironment: key role for myeloid cells in antitumor immunity, Radiother. Oncol. 174 (2022) 158–167, https://doi.org/10.1016/j.radonc.2022.07.014.
[8] S. Glück, B. Guey, M.F. Gulen, K. Wolter, T.-W. Kang, N.A. Schmacke, et al., Innate immune sensing of cytosolic chromatin fragments through cgas promotes senescence, Nat. Cell Biol. 19 (9) (2017) 1061–1070, https://doi.org/10.1038/ncb3586.
[9] L. Chibaya, J. Snyder, M. Ruscetti, Senescence and the tumor-immune landscape: implications for cancer immunotherapy, Semin. Cancer Biol. 86 (Pt 3) (2022) 827–845, https://doi.org/10.1016/j.semcancer.2022.02.005.
[10] C.-W. Liu, P.-H. Chen, T.-J. Yu, K.-J. Lin, L.-C. Chang, Wwox modulates ros-dependent senescence in bladder cancer, Molecules 27 (21) (2022), https://doi.org/10.3390/molecules27217388.
[11] G. Fu, Y. Wu, G. Zhao, X. Chen, Z. Xu, J. Sun, et al., Activation of cgas-sting signal to inhibit the proliferation of bladder cancer: the immune effect of cisplatin, Cells 11 (19) (2022), https://doi.org/10.3390/cells11193011.
[12] D. Saul, R.L. Kosinsky, E.J. Atkinson, M.L. Doolittle, X. Zhang, N.K. LeBrasseur, et al., A new gene set identifies senescent cells and predicts senescence-associated pathways across tissues, Nat. Commun. 13 (1) (2022) 4827, https://doi.org/10.1038/s41467-022-32552-1.
[13] B. Salomé, J.P. Sfakianos, D. Ranti, J. Daza, C. Bieber, A. Charap, et al., Nkg2a and hla-E define an alternative immune checkpoint Axis in bladder cancer, Cancer Cell 40 (9) (2022), https://doi.org/10.1016/j.ccell.2022.08.005.
[14] Q. Duan, H. Zhang, J. Zheng, L. Zhang, Turning cold into hot: firing up the tumor microenvironment, Trends Cancer 6 (7) (2020) 605–618, https://doi.org/10.1016/j.trecan.2020.02.022.
[15] D. Maeser, R.F. Gruener, R.S. Huang, Oncopredict: an R package for predicting in vivo or cancer patient drug response and biomarkers from cell line screening data, Briefings Bioinf. 22 (6) (2021), https://doi.org/10.1093/bib/bbab260.
[16] M.E. Winerdal, D. Krantz, C.A. Hartana, A.A. Zirakzadeh, L. Linton, E.A. Bergman, et al., Urinary bladder cancer Tregs suppress Mmp 2 and potentially regulate invasiveness, Cancer Immunol. Res. 6 (5) (2018) 528–538, https://doi.org/10.1158/2326-6066.CIR-17-0466.
[17] A. Lin, J. Zhang, P. Luo, Crosstalk between the msi status and tumor microenvironment in colorectal cancer, Front. Immunol. 11 (2020) 2039, https://doi.org/10.3389/fimmu.2020.02039.
[18] M. Palmeri, J. Mehnert, A.W. Silk, S.K. Jabbour, S. Ganesan, P. Popli, et al., Real-world application of tumor mutational burden-high (Tmb-High) and microsatellite instability (msi) confirms their utility as immunotherapy biomarkers, ESMO Open 7 (1) (2022) 100336, https://doi.org/10.1016/j.esmoop.2021.100336.
[19] K.-C. Huang, D. Chanda, S. McGrath, V. Dixit, C. Zhang, J. Wu, et al., Pharmacologic activation of sting in the bladder induces potent antitumor immunity in non-muscle invasive murine bladder cancer, Mol. Cancer Therapeut. 21 (6) (2022) 914–924, https://doi.org/10.1158/1535-7163.MCT-21-0780.
[20] W. Li, L. Lu, J. Lu, X. Wang, C. Yang, J. Jin, et al., Cgas-sting-mediated DNA sensing maintains Cd8 T cell stemness and promotes antitumor T cell therapy, Sci. Transl. Med. 12 (549) (2020), https://doi.org/10.1126/scitranslmed.aay9013.
[21] T.M. Loo, K. Miyata, Y. Tanaka, A. Takahashi, Cellular senescence and senescence-associated secretory phenotype via the cgas-sting signaling pathway in cancer, Cancer Sci. 111 (2) (2020) 304–311, https://doi.org/10.1111/cas.14266.
[22] G.V. Sharonov, E.O. Serebrovskaya, D.V. Yuzhakova, O.V. Britanova, D.M. Chudakov, B cells, plasma cells and antibody repertoires in the tumour microenvironment, Nat. Rev. Immunol. 20 (5) (2020) 294–307, https://doi.org/10.1038/s41577-019-0257-x.
[23] B. Farhood, M. Najafi, K. Mortezaee, Cd8 cytotoxic T lymphocytes in cancer immunotherapy: a review, J. Cell. Physiol. 234 (6) (2019) 8509–8521, https://doi.org/10.1002/jcp.27782.
[24] C. Cui, J. Wang, E. Fagerberg, P.-M. Chen, K.A. Connolly, M. Damo, et al., Neoantigen-driven B cell and Cd4 t follicular helper cell collaboration promotes anti-tumor Cd8 T cell responses, Cell 184 (25) (2021), https://doi.org/10.1016/j.cell.2021.11.007.
[25] S. Crotty, Follicular helper Cd4 T cells (tfh), Annu. Rev. Immunol. 29 (2011) 621–663, https://doi.org/10.1146/annurev-immunol-031210-101400.

[26] W. Song, J. Craft, T follicular helper cell heterogeneity: time, space, and function, Immunol. Rev. 288 (1) (2019) 85–96, https://doi.org/10.1111/imr.12740.
[27] S. Yan, Y. Zhang, B. Sun, The function and potential drug targets of tumour-associated Tregs for cancer immunotherapy, Sci. China Life Sci. 62 (2) (2019) 179–186, https://doi.org/10.1007/s11427-018-9428-9.
[28] C. Luchini, F. Bibeau, M.J.L. Ligtenberg, N. Singh, A. Nottegar, T. Bosse, et al., Esmo recommendations on microsatellite instability testing for immunotherapy in cancer, and its relationship with Pd-1/Pd-L1 expression and tumour mutational burden: a systematic review-based approach, Ann. Oncol. 30 (8) (2019) 1232–1243, https://doi.org/10.1093/annonc/mdz116.
[29] M. Pollak, The insulin and insulin-like growth factor receptor family in neoplasia: an update, Nat. Rev. Cancer 12 (3) (2012) 159–169, https://doi.org/10.1038/nrc3215.
[30] Y. Neuzillet, E. Chapeaublanc, C. Krucker, L. De Koning, T. Lebret, F. Radvanyi, et al., Igf1r activation and the in vitro antiproliferative efficacy of Igf1r inhibitor are inversely correlated with Igfbp5 expression in bladder cancer, BMC Cancer 17 (1) (2017) 636, https://doi.org/10.1186/s12885-017-3618-5.
[31] X. Long, W. Xiong, X. Zeng, L. Qi, Y. Cai, M. Mo, et al., Cancer-associated fibroblasts promote cisplatin resistance in bladder cancer cells by increasing igf-1/erβ/bcl-2 signalling, Cell Death Dis. 10 (5) (2019) 375, https://doi.org/10.1038/s41419-019-1581-6.
[32] X. Mao, J. Xu, W. Wang, C. Liang, J. Hua, J. Liu, et al., Crosstalk between cancer-associated fibroblasts and immune cells in the tumor microenvironment: new findings and future perspectives, Mol. Cancer 20 (1) (2021) 131, https://doi.org/10.1186/s12943-021-01428-1.
[33] M. Desbois, Y. Wang, Cancer-associated fibroblasts: key players in shaping the tumor immune microenvironment, Immunol. Rev. 302 (1) (2021) 241–258, https://doi.org/10.1111/imr.12982.

## Abbreviation

*Bladder cancer:* BLCA
*Stimulator of interferon genes:* STING
*cyclic GMP-AMP:* cGAMP
*cyclic GMP-AMP synthase:* cGAS
*I interferon:* IFN
*senescence-associated secretory phenotype:* SASP
*the cancer genome map::* TCGA
*Gene Expression Omnibus:* GEO
*differentially expressed genes:* DEGs
*fold change:* FC
*cumulative distribution function:* CDF
*human leukocyte antigen:* HLA
*overall survival:* OS
*Disease-specific survival:* DSS
*least absolute shrinkage and selector operation:* LASSO
*Kaplan-Meier:* K-M
*Tumor Mutation Burden:* TMB
*microsatellite instability:* MSI
*Maximum Neighborhood Component:* MNC
*time-dependent receiver operating characteristic:* time-ROC
*Human Protein Atlas:* HPA
*target genes:* TGs
*progression-free survival:* PFS
*T cell regulatory:* Tregs
*T cell follicular helper:* TFH